Investigation on thermal response in fretting sliding with the consideration of plastic dissipation, surface roughness and wear

Fei Shen, Kun Zhou*

School of Mechanical and Aerospace Engineering, Nanyang Technological University, 50 Nanyang Avenue, Singapore 639798, Singapore

ARTICLE INFO

ABSTRACT

This study investigates the thermal response of titanium alloy fretting sliding through a numerical approach with the consideration of the friction dissipation, plastic dissipation, surface roughness and wear. The fretting sliding of a cylindrical pad on a specimen with surface roughness is modeled to predict the temperature distribution, the evolution of the wear profile, and the fields of surface and subsurface stresses. Specifically, a thermo-elasto-plastic constitutive model considering the thermal-induced softening of material properties is developed to evaluate the contact pressure and the tangential stress on the surfaces as well as the subsurface stresses in the contacting components. The friction and plastic energy dissipations function together as the heat source to cause the temperature rise in the contact zone. A modified Archard model is used to predict the wear profile of the contact surface and change the contact geometry. The models are then incorporated in the finite element analysis of the fretting sliding to evaluate the thermal response. The influences of the plastic dissipation and the surface roughness on the temperature rise in the fretting sliding are discussed.

1. Introduction

Fretting is the oscillatory motion of two contacting bodies under small relative displacements. The friction behavior on the contact surfaces causes material damage including wear and fatigue [1–3]. The formation of wear debris is mainly attributed to the plastic deformation, oxidation, and subsequent detachment of surface and near-surface materials [4–6]. The cyclic subsurface stresses induced by the oscillatory motion could give rise to the initiation and propagation of fatigue cracks in the contacting components. Besides the material damage, the energies from the friction and the plastic deformations are dissipated in the contact zone and thus cause the temperature rise during the fretting sliding process [7,8].

Temperature affects mechanical and thermal properties of materials including the Young's modulus, yield limit, density, specific heat and thermal conductivity. The thermal-induced softening leads to the reduction of the surface and subsurface stresses. The coefficient of friction is also influenced by the temperature in the contact zone [9]. High temperature encourages the formation of oxide debris serving as the third body between the contacting components [8]. The wear rates of the carbon steel and titanium alloy were observed to increase firstly with the increasing temperature and then decrease rapidly when it exceeded the transition temperature [10,11]. The material wear alters the contact geometry progressively and results in the variation of the surface and subsurface stresses [12–15]. Therefore, the friction and

plastic energy dissipations are thus affected by the wear of surface materials.

Previous researches have focused on the investigation of the thermal response resulting from the energy dissipation in fretting sliding [16–19]. A number of factors were reported to influence the temperature rise in the contact zone, which can be classified into three categories. They are the loading conditions (the contact force, the relative slip displacement or friction force, and the loading frequency), the interfacial properties (the contact geometry, the surface roughness, and the coefficient of friction) and the mechanical and thermal properties of materials. The factors determine the distributions of the plastic strain, the surface stresses (contact pressure and tangential stress) and the subsurface stresses in the components, thus influencing the energy dissipation and the temperature rise. Conversely, some factors including the contact geometry, the coefficient of friction and the material properties are also changed gradually due to the temperature increase and the material wear. Therefore, there are strong interactions among the temperature, the wear behavior and the factors in fretting sliding [9,20].

Since it is difficult to measure the temperature rise in the contact zone, numerical methods have been widely used to model the fretting friction behavior and predict the temperature distribution. Jaeger [21] firstly proposed a moving heat source model to predict the temperature rise in a semi-infinite body. Based on the pioneer work, numbers of analytical methods were developed to investigate the effects of the types and shapes of the heat source models on the temperature rise [19,22]. The analytical methods have the advantage of low computational cost

---

but are only applicable to the simple fretting conditions. Furthermore, the change of the contact surface geometry caused by the wear cannot be considered. In order to overcome the limitations, the finite element-based methods have been applied to provide more realistic modeling of the friction-induced temperature rise [18]. Jin et al. [8] developed a finite element model considering the wear to study the role of wear on the temperature field in the fretting contact of 304 stainless steel. Recently, the effect of the surface roughness on the temperature distribution in a steel-on-steel fretting contact was investigated by a similar method without the consideration of wear [23]. The surface roughness has influences on the distributions of the surface and subsurface stresses, the wear behavior and the temperature rise [23–26].

The aforementioned approaches considered the friction energy dissipation as the unique heat source. The plastic dissipation was ignored in the simulations. It is reasonable under some conditions that small or even no plastic deformation occurs. However, the plastic dissipation should be included in the heat source as the plastic deformation is significant. The self-heating behavior induced by the plastic dissipation has been investigated under cyclic loading for polymeric and metallic materials [27–29]. In the study, the plastic dissipation is considered as a volumetric heat source generated in the loading process associated with the plastic deformation. In the simulation of fretting sliding with the consideration of the surface roughness, the contact between the components occurs on small area around several peaks of the surfaces, leading to high surface stresses and large plastic strain at the peaks [23]. Therefore, the plastic dissipation should be considered together with the friction energy dissipation in the modeling of the thermal response in fretting sliding.

This study develops a numerical approach to predict the temperature rise in the titanium alloy fretting sliding with a cylinder-on-flat contact configuration. The friction dissipation, plastic dissipation, surface roughness and wear are considered in the approach. A thermo-elasto-plastic constitutive model is developed to evaluate the contact pressure and the tangential stress on the surfaces as well as the subsurface stresses. The thermal-induced softening of the material properties including the Young's modulus and the yield limit is taken into account. Both the plastic and friction dissipations are considered as the heat source. A modified Archard law is used to model the wear-induced variation of the contact geometry. The temperature-dependent wear coefficient is included to consider the effect of the temperature on the wear rate. The models are incorporated in the coupled temperature-displacement finite element analysis of the fretting sliding, in which the surface roughness of the contact surface is considered. The temperature rise, the wear profile, and the surface and subsurface stresses are obtained using the developed approach. The influences of the plastic dissipation and the surface roughness on the temperature rise are also investigated.

2. Theoretic models

2.1. Thermo-elasto-plastic constitutive model

A thermo-elasto-plastic constitutive model is developed to predict the distributions of the surface and subsurface stresses in fretting sliding. Due to the contact between the components, the stress concentration usually causes the plastic deformation in the contact zone. Furthermore, the friction- and plastic-induced heating over the contact surfaces softens the material properties. Therefore, the elasto-plastic behavior and the thermal-induced softening of metallic materials are considered in the model.

The constitutive model is developed on the basis of the Chaboche plasticity model [30–33] which takes the isotropic hardening and the nonlinear kinematic hardening rules into account. The total strain under small strain assumption is decomposed to three strain tensors:

$$\varepsilon = \varepsilon^{\mathrm{e}} + \varepsilon^{\mathrm{p}} + \varepsilon^{\mathrm{th}}, \tag{1}$$

where the tensors ε, ε^{e}, ε^{p} and $\varepsilon^{\mathrm{th}}$ are the total strain, elastic strain, plastic strain and thermal strain, respectively. The elastic law including the effect of the temperature on the material properties is given as

$$\sigma = \mathbf{C}^{\mathrm{e}}(T) : \varepsilon^{\mathrm{e}}, \tag{2}$$

where $\mathbf{C}^{\mathrm{e}}(T)$ is the elastic modulus tensor that can be described by the temperature-dependent Young's modulus $E(T)$ and Poisson's ratio ν. The influence of the temperature on the Poisson's ratio is not considered in this study. For metallic materials, the Young's modulus commonly exhibits a linear relationship with the temperature:

$$E(T) = E_{\mathrm{s}}(T - T_0) + E_0, \tag{3}$$

where E_0 is the modulus at the temperature T_0. The material parameter E_{s} is the slop of the linear relationship, which is a negative value due to the thermal-induced softening of the Young's modulus.

The von Mises yield function is given as

$$F = \|\mathbf{s} - \mathbf{X}\| - \sigma_{\mathrm{y}}(T) = \sqrt{\frac{3}{2}(\mathbf{s} - \mathbf{X}) : (\mathbf{s} - \mathbf{X})} - \sigma_{\mathrm{y}}(T), \tag{4}$$

where $\mathbf{s}$ and $\mathbf{X}$ are the deviatoric Cauchy stress and the back stress, respectively. The back stress represents the motion of the yield surface and its evolution is considered in the kinematic hardening rule. The yield limit $\sigma_{\mathrm{y}}(T)$ is the size of the yield surface. The isotropic hardening rule controlling the evolution of the yield limit associated with the plastic strain is not considered in the study. Thus the yield limit is regarded as a function of only the temperature, which is expressed as

$$\sigma_{\mathrm{y}}(T) = \sigma_{\mathrm{ys}}(T - T_0) + \sigma_{\mathrm{y0}}, \tag{5}$$

where σ_{y0} is the yield limit at the temperature T_0 and σ_{ys} is a material parameter with a negative value. Based on the yield function, the plastic flow can be derived as

$$\dot{\varepsilon}^{\mathrm{p}} = \dot{\lambda}\frac{\partial F}{\partial \sigma} = \frac{3}{2}\dot{\lambda}\frac{\mathbf{s} - \mathbf{X}}{\|\mathbf{s} - \mathbf{X}\|}, \tag{6}$$

where the term λ is the plastic multiplier. The nonlinear kinematic hardening rule is expressed as

$$\mathbf{X} = \sum_{i=1}^{K} \mathbf{X}_i, \tag{7}$$

$$\dot{\mathbf{X}}_i = \frac{2}{3}C_i(T)\dot{\varepsilon}^{\mathrm{p}} - \gamma_i(T)\mathbf{X}_i\dot{\lambda}, \tag{8}$$

where K is the number of the back stress, $C_i(T)$ and $\gamma_i(T)$ are hardening-related material parameters.

The thermal stain in Eq. (1) is determined by the increment of the temperature and the thermal expansion coefficient θ:

$$\varepsilon^{\mathrm{th}} = \theta(T - T_0). \tag{9}$$

2.2. Heat transfer model

The heat source in the fretting sliding includes the dissipations from the friction energy and the plastic energy. It is noted that the friction energy dissipated on the contact surfaces is regarded as a surface heat flux and the plastic dissipation is treated as a volumetric heat source. The heat transfer equation for a material with isotropic thermal properties is given as

$$\rho c \frac{\partial T}{\partial t} = \nabla \cdot (k\nabla T) + \sigma : \dot{\varepsilon}^{\mathrm{p}}, \tag{10}$$

where ρ, c and k are the density, heat capacity and conductivity, respectively. The term $\sigma : \dot{\varepsilon}^{\mathrm{p}}$ is the rate of the dissipated energy density due to the plastic deformation. The energy stored in the material due to the kinematic hardening is negligible [34]. On the contact surfaces, the thermal boundary condition considering the heat flux due to the frictional energy dissipation is given as

$$-nk\nabla T = \beta\tau\dot{\delta} - h(T - T_0), \tag{11}$$
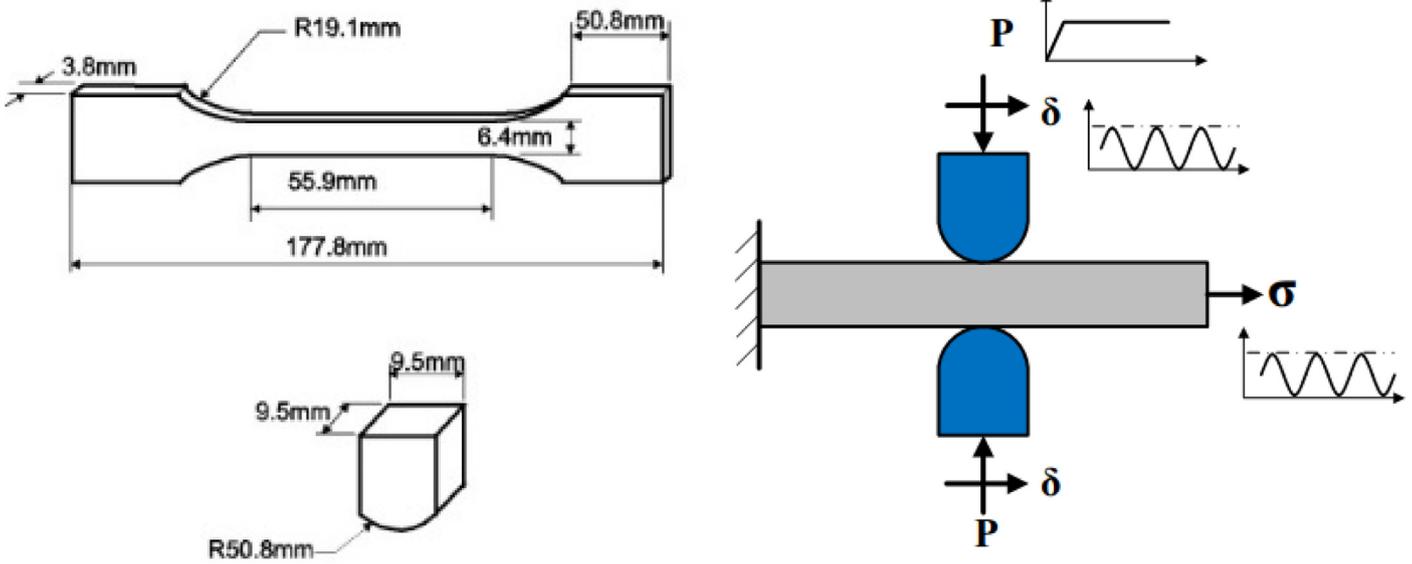
Fig. 1. Schematic diagram of the fretting contact configuration.

where n is the surface normal direction, h is the natural convection coefficient, τ is the frictional stress, $\dot{\delta}$ is the slip rate, and $\tau\dot{\delta}$ is the total friction work. The coefficient β is the weighting factor for the distribution of the friction work between the interacting surfaces. The common value of $\beta = 0.5$ is used, indicating that the generated heat is partitioned equally into the pad and the specimen.

2.3. Modified Archard model

A modified Archard model is used to consider the change of contact surface geometries caused by the material wear. In the original model, the wear volume is related to the contact pressure and the relative slip distance [35–38]. In order to consider the effect of the temperature on the wear behavior, the temperature-dependent wear coefficient $\Phi(T)$ is used in this study. Furthermore, the contact pressure is varied in fretting sliding and thus the integral form of the model is used. For a given point at the position x on the two-dimensional contact surface, the wear depth at time t is expressed as

$$d(x, t, T) = \phi(T) \int_{t=0}^{t} p(x, t) \mathrm{d}\delta(x, t),\tag{12}$$

where $p(x, t)$ is the contact pressure at the point and $\mathrm{d}\,\delta(x, t)$ is the increment of the relative slip displacement.

3. Computational methodology

The cylinder-on-flat contact configuration in the fretting fatigue experiments [39,40] is used in this study. Two cylindrical pads with the radius of 50.8 mm contact with a flat specimen under the normal force of 1334 N, as shown in Fig. 1. The cyclic slip displacement is also applied on the two pads. One edge of the specimen is fixed and the cyclic stress with the same frequency as that of the slip displacement is applied on the other edge. The pads and the specimen are made of Ti-6Al-4 V.

3.1. Surface roughness modeling

The top surface of the specimen is modeled as a sinusoidal function to represent the rough morphology of the surface. The wave length and the height amplitude are two parameters governing the surface shape. The width of the contact area is around 0.9 mm as the surface roughness
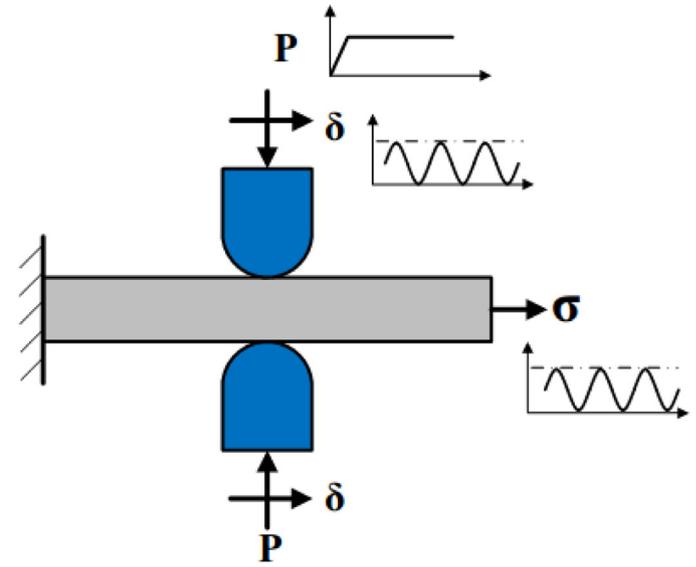
is not considered [12]. In the study, the wave length is set to be 0.2 mm based on the experimental observation in the fretting sliding experiment [23]. Two height amplitudes ($R_a = 6$ and $12.5\,\mu$m) and the smooth surface condition are considered to study the effect of surface roughness on the temperature rise. The width of the rough contact surface is limited to 3 mm which is much larger than the slip displacement applied on the pad. The roughness of the cylindrical surface on the pad is not considered because the friction and the wear on the specimen surface are dominant as reported in fretting wear experiments [40].

3.2. Coupled temperature-displacement finite element analysis of fretting sliding

Half of the fretting contact configuration is modeled using the nonlinear finite element package ABAQUS according to the symmetric feature. The 4-node, coupled displacement-temperature plane strain element (CPE4T) is used to calculate the displacement and temperature distributions. In order to capture the severe stress concentration, the fine mesh (around 10 μm in dimension) is generated in the contact zone, especially on the rough surface of the specimen and the cylindrical surface of the pad as shown in Fig. 2. The mesh far away from the contact zone is coarse to save the computation cost. The origin of the coordinate system is set at the center of the top surface of the specimen. The contact between the pad and the specimen is defined using the master-slave algorithm. The rough surface of the specimen is defined as the slave surface and part of the circular surface of the pad is defined as the master surface. The initial adjustment of the nodes on the slave surface is conducted to clear the gap between the pad and the specimen. Coulomb friction model is used to calculate the frictional stress. It is noted that the surface roughness and the temperature affects the coefficient of friction. Usually, rougher surface and lower temperature lead to higher coefficient of friction. According to the fretting wear experiments of Ti-6Al-4 V [9,41], the friction coefficient is determined to be a linear relationship with the temperature in a range from 25 to 300 °C:

$$\mu(T) = 0.8 - 8.84 \times 10^{-4}(T - 25).\tag{13}$$

The surface roughnesses of the contact surfaces were changed from around 7 to 18.7 μm in the testing due to different coatings, which are similar with the roughness conditions considered in the simulation. Therefore, the coefficient of friction in Eq. (13) is used to model the friction behavior of Ti-6Al-4 V fretting sliding. The initial temperature
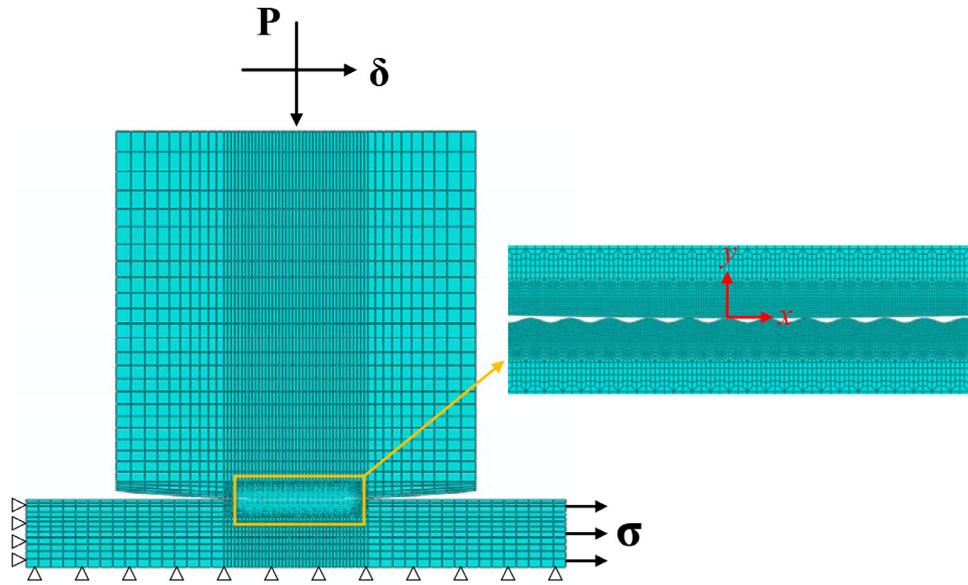
Fig. 2. Finite element model of the fretting sliding between the pad and specimen with the consideration of the surface roughness.

Table 1
Temperature-dependent physical properties of Ti-6Al-4 V [42].

Temperature (°C)	Thermal conductivity (W/(m °C))	Specific heat (J/(kg °C))	Density (kg/m³)
25	7	546	4420
100	7.45	562	4406
200	8.75	584	4395
300	10.15	606	4381
400	11.35	629	4366
500	12.6	651	4350
600	14.2	673	4336
700	15.5	694	4324

of the pad and the specimen is set as 25 °C. The heat convection boundary condition with the coefficient of 100 W/(m² °C) is applied on the two contact surfaces of the pad and specimen. The thermal expansion coefficient is set as $\theta = 8.7 \times 10^{-6}$. The temperature-dependent physical properties of Ti-6Al-4 V including the thermal conductivity, specific heat and density are listed in Table 1 [42].

The loads are applied on the finite element model through three steps. In the first step, a small normal contact load is applied on the pad to establish the contact. Then it increases to the experimental value (208 N/mm) in the second step, and remains unchanged in the third step. The cyclic slip displacement and the in-phase cyclic stress are both applied in the third step. The frequency and the slip displacement of the fretting sliding are $f = 200$ Hz and $\delta = 40\ \mu$m, respectively. The maximum stress value is 550 MPa and the stress ratio is 0.03.

3.3. Determination of the material parameters and the wear coefficient

The uniaxial tensile stress-strain data of Ti-6Al-4 V under different temperatures [43] are used to determine the material parameters in the thermo-elasto-plastic constitutive model. The parameters E_0, E_s, σ_{y0}, and σ_{ys} are determined through the Young's moduli and the yield limits obtained at various temperatures. The method of the parameter determination for the nonlinear kinematic hardening rule was presented in the previous study [12]. For the material Ti-6Al-4 V, two components of the back stress are adopted ($K = 2$). The parameters C_1, C_2, γ_1, and γ_2 obtained at $T_0 = 25$ °C can be used to reproduce the stress-strain data at other four temperatures. Fig. 3 shows the experimental points and the fitting curves under different temperatures. The material properties and model parameters in the constitutive model for Ti–6Al–4 V are listed in Table 2.
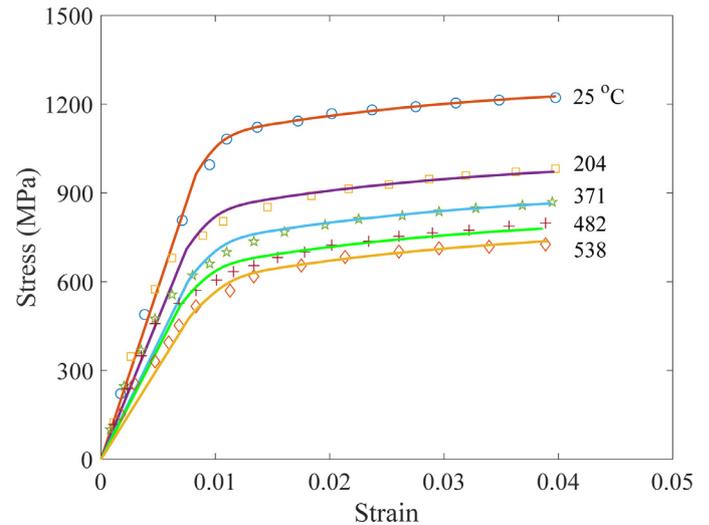
Fig. 3. Experimental stress–strain data of Ti–Al–4 V and fitting curves under different temperatures.

The temperature-dependent wear coefficient is obtained using the experimental results of Ti-6Al-4 V wear testing conducted by Wang et al. [11]. It was found that a severe-to-mild wear transition occurred with an increase in temperature. Below the critical transition temperature (around 350 °C), the wear coefficient increased linearly with the temperature. Therefore, the linear relationship between the wear coefficient
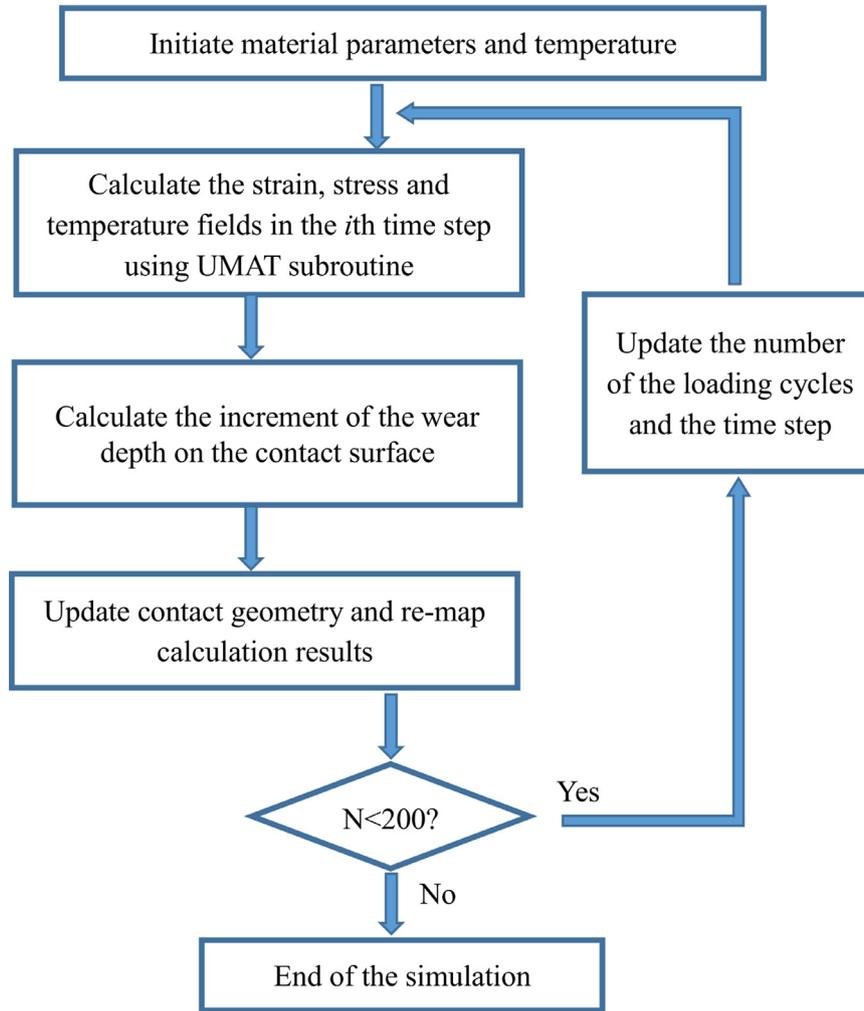
Fig. 4. Simplified flowchart of the numerical implementation.

Table 2
Parameters of the thermo-elasto-plastic constitutive model for Ti–6Al–4 V.

E_0(MPa)	E_s(MPa/°C)	σ_{y0}(MPa)	σ_{ys}(MPa/°C)	v
114,582	−97.6	927.3	−0.908	0.34

C_1(MPa)	C_2(MPa)	γ_1	γ_2	T_0
136,500	8100	1050	45	25

and the temperature is used in the simulation:

$$\phi(T) = 3.06 \times 10^{-7} + 5 \times 10^{-10}(T - 25). \tag{14}$$

It is noted that the surface roughness condition of the wear testing specimen influences the measured wear coefficient. Generally, the wear coefficient increases with the increase of the surface roughness. However, the information of the surface roughness in the wear testing is unavailable. For the simplicity, the roughness-independent wear coefficient is used to model the material wear on the contact surface.

3.4. Numerical implementation

The aforementioned theoretic models are incorporated into the coupled temperature-displacement finite element analysis of the fretting sliding. As shown in Fig. 4, the numerical implementation includes the calculation of the stress and stain distributions, the evaluation of the temperature rise, and the prediction of the wear profile evolution on the contact surfaces.

The thermo-elasto-plastic constitutive model is implemented using the user subroutine UMAT in the software package ABAQUS to obtain the elastic and plastic strains, surface and subsurface stresses under certain temperature. The implicit return mapping algorithm is applied to calculate the increments of the variables based on the results at the previous time steps. The stress and other solution-dependent variables are updated at the end of the current time step. In the coupled temperature-displacement analysis, the variable RPL representing the volumetric heat generation per unit time caused by the plastic dissipation is needed to be updated in the subroutine. Based on Eq. (10), the increment of RPL is described as $\Delta(RPL) = \sigma : \Delta\varepsilon^p$, where the $\Delta\varepsilon^p$ is the increment of the plastic strain. After the calculation of the stress and strain fields, the increment of RPL can be provided at the end of the time step. It is noted that the heat generation due to the friction energy dissipation is handled by the setting of the contact property in the software. According to the plastic work and the friction work, the increment of the temperature is calculated using the heat transfer model.

In the subroutine UMAT, the consistent tangent modulus $d\sigma/d\varepsilon$ needs to be updated at the end of the time step. In the coupled temperature-displacement analysis, other three variables related to the temperature also should be provided in the simulation, which are the variation of the stress increment with respect to the temperature $d\sigma/dT$, the variation of the plastic work with respect to the strain increments $d(RPL)/d\varepsilon$, and the variation of the plastic work with respect to the tem-

perature d(RPL)/dT. Using the chain rule, the last two derivatives are written as

$$\frac{\mathrm{d}(RPL)}{\mathrm{d}\varepsilon} = \frac{\mathrm{d}\boldsymbol{\sigma}}{\mathrm{d}\varepsilon} : \dot{\boldsymbol{\varepsilon}}^p + \boldsymbol{\sigma} : \frac{\mathrm{d}\dot{\boldsymbol{\varepsilon}}^p}{\mathrm{d}\varepsilon}, \tag{15}$$

$$\frac{\mathrm{d}(RPL)}{\mathrm{d}T} = \frac{\mathrm{d}\boldsymbol{\sigma}}{\mathrm{d}T} : \dot{\boldsymbol{\varepsilon}}^p + \boldsymbol{\sigma} : \frac{\mathrm{d}\dot{\boldsymbol{\varepsilon}}^p}{\mathrm{d}T}. \tag{16}$$

The modified wear model is implemented using the user subroutine UMESHMOTION. Based on the temperature distribution on the contact surfaces, the wear coefficient is obtained using Eq. (14). According to the contact pressure and the relative slip displacement, the increment of the wear depth for a given node on the contact surface during the ith time step is calculated by

$$\Delta d_i = \phi(T) p_i \Delta \delta_i, \tag{17}$$

where p_i and $\Delta \delta_i$ are the contact pressure at the end of the time step and the increment of the relative slip during the time step, respectively. Then the contact geometry is changed through moving the contact node a distance of Δd_i in the direction opposite to the normal direction at the end of the time step. After that, the result variables are re-mapped to the new position. Through repeating the aforementioned steps, the distributions of the temperature and stresses are calculated with the consideration of the evolution of the contact surface geometry caused by wear. The maximum number of cycles is set as 200 in the study.

4. Results and discussion

4.1. Distributions of the temperature, wear profile, and stresses

The distributions of the temperature, the wear profile, and the surface and subsurface stresses are obtained using the developed numerical approach. The simulation case with the surface roughness of 12.5 μm is taken as the example to illustrate the results. Fig. 5(a) shows the temperature filed in the contact zone after 200 cycles under the loading condition of $f = 200$ Hz and $\delta = 40$ μm. The temperature rise mainly concentrates in a small region around the contact surface, especially at three surface peaks. The difference between the maximum temperatures at the pad and the specimen is insignificant due to the equally partition of the friction energy into both components. The maximum temperature of around 53 °C locates at the surface peak with the position of $x = 0.38$ mm. Fig. 5(b) depicts the distributions of the temperature rise on the rough surface of the specimen after three numbers of loading cycles. The contact between the pad and the specimen occurs at several peaks and thus the friction and plastic energies dissipate over the area near the peaks. Therefore, the temperature at the surface peaks is larger than that at the valley. The maximum temperature rise after the first cycle is around 50 °C, which is the combined contribution of the friction and plastic dissipations during the cycle. As the number of the cycles increases up to 200, the maximum temperature only increases by around 3 °C.

The contact geometry changes due to the material wear on the rough surface. Fig. 6 shows the distributions of the wear depth on the rough surface of the specimen after 30 and 200 cycles. With the consideration of the surface roughness, the wear occurs in several discrete zones. It is quite different from the results obtained under the condition of the smooth surface [12,13]. If the surface roughness is not considered, the wear profile exhibits a Hertzian shape due to the similar distribution of the contact pressure on the surface. As shown in Fig. 6, the total width of the worn scars remains unchanged as the number of loading cycles increases from 30 to 200. The maximum wear depth after 200 cycles is around 0.7 μm which is much smaller than the element height. However, the surface and subsurface stresses are influenced by the change of the contact geometry as the materials at the surface peaks are worn away.
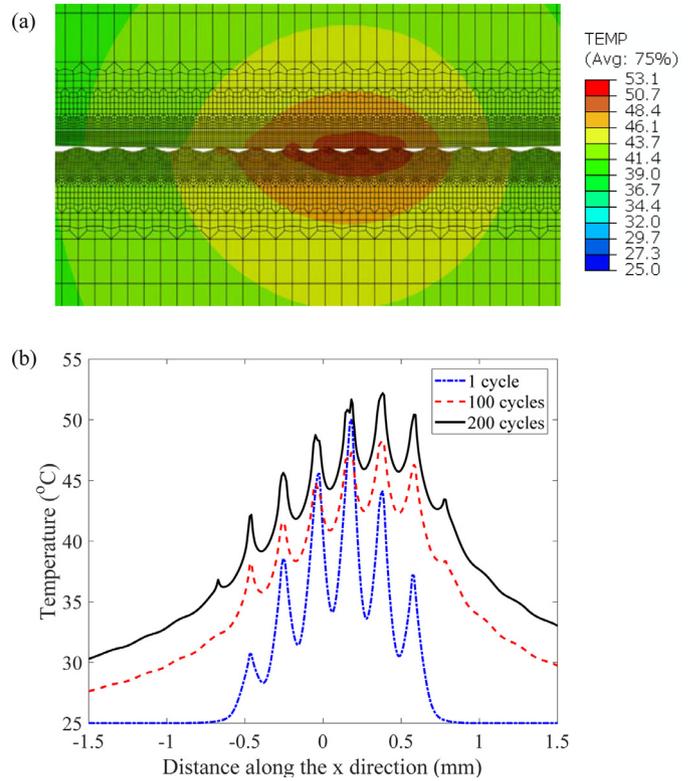
Fig. 5. (a) Temperature field in the contact zone after 200 cycles for the simulation case with $R_a = 12.5$ μm. (b) Distributions of the temperature on the rough surface of the specimen after 1, 100 and 200 cycles.
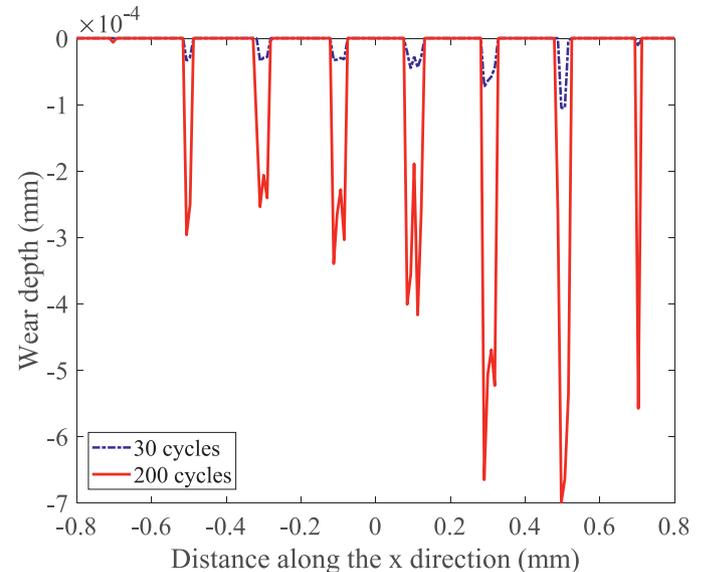
Fig. 6. Distributions of the wear depth on the rough surface of the specimen for the simulation case with $R_a = 12.5$ μm after 30 and 200 cycles.

Fig. 7 shows the distributions of the accumulated plastic strain, the contact pressure and the Mises stress on the rough surface of the specimen. The plastic deformation also occurs at the surface peaks. It is worth noted that the maximum accumulated plastic strain at the surface peak is about 0.45 in the first cycle, indicating that the plastic dissipation should be considered in the simulation. The significant plastic dissipation leads to the rapid increase of the temperature as shown in Fig. 5(b). However, the increment of the accumulated plastic strain reduces significantly to
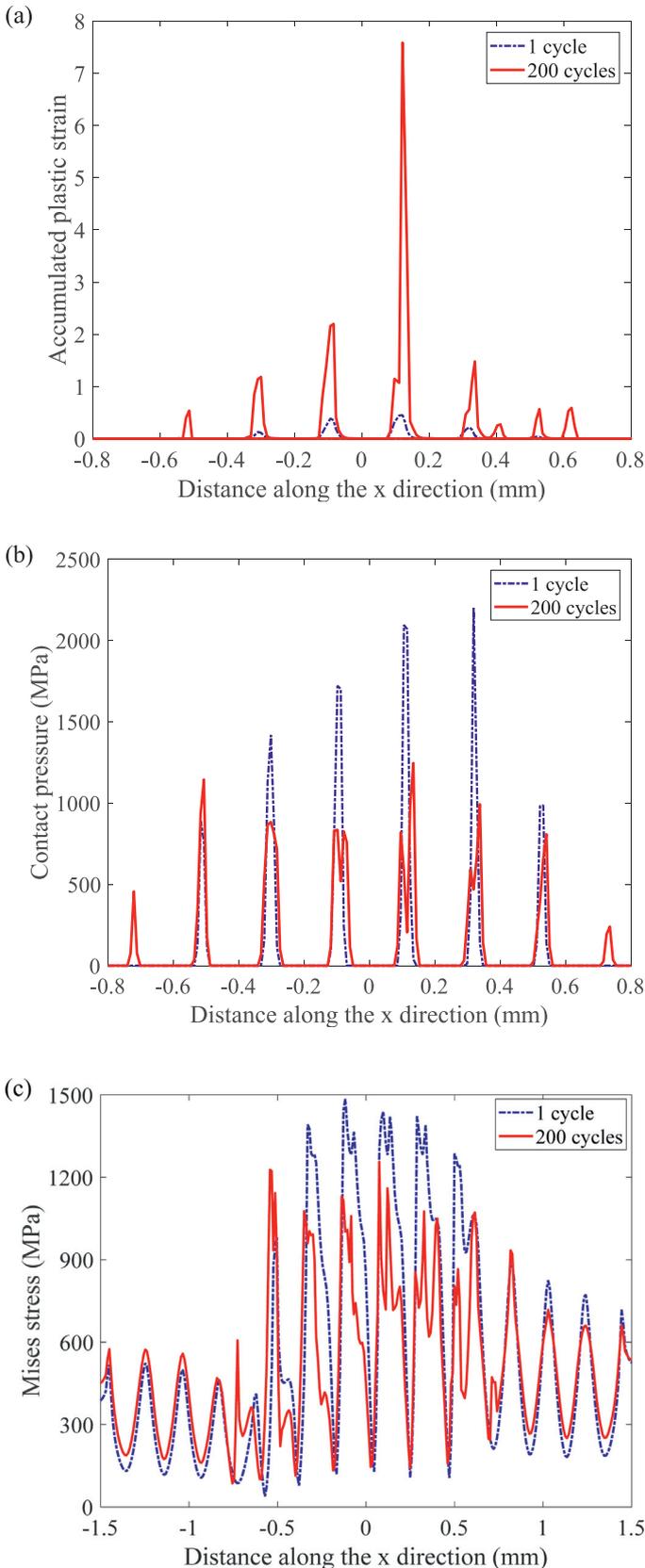
Fig. 7. Distributions of (a) the accumulated plastic strain, (b) the contact pressure, and (c) the Mises stress on the rough surface of the specimen for the simulation case with $R_a = 12.5 \, \mu$m.

around 0.05 in the subsequent cycles due to the material hardening. The initial distribution of the contact pressure no longer exhibits a Hertzian shape, as shown in Fig. 7(b). The contact force is carried by the materials at six peaks on the rough surface and the total contact area is much smaller than that in the condition of the smooth surface. Therefore, the contact pressure is high at the contacting peaks in the first cycle. Because of the worn of materials at the peaks and the temperature rise, the contact pressure drops significantly from around 2000 to 1000 MPa. More peaks begin to contact with the pad and carry the contact force. The similar trend is also observed in the distributions of the Mises stress as shown in Fig. 7(c). High Mises stress occurs at the peaks located at the position of $-0.5 < x < 0.5$ mm and its value decreases with the increase of the number of loading cycles.

4.2. Effects of the plastic and friction dissipations on the temperature rise

The results in the previous subsection are obtained using the approach considering both the friction dissipation and the plastic dissipation. The effects of both energies on the temperature rise are combined together in the simulation. In order to unveil their separate effects, two simulations with $R_a = 12.5 \, \mu$m are conducted in which the plastic dissipation and the friction dissipation are individually considered, respectively.

Fig. 8(a) shows the evolutions of the temperature on the rough surface of the specimen obtained by two approaches. As only the plastic energy is treated as the heat source, a rapid increase of the temperature up to about 40 °C is observed in the first loading cycle. After that the temperature gradually reduces to a stable value of around 26 °C. Even though the plastic deformation still exists in the subsequent cycles, the plastic energy is much smaller than that in the first cycle. In the simulation, the increment of the accumulated plastic strain in the first cycle is about 0.4 which is one order of magnitude larger than that in the subsequent cycle. The heat convection on the surface is dominant compared with the heat input from the plastic dissipation, causing the reduction of the temperature. If the plastic dissipation is not considered, the friction energy causes the maximum temperature to increase with the increase of the number of loading cycles. In the first cycle, the maximum temperature is around 36 °C less that the result in the case of considering plastic dissipation only. Another phenomenon is that there are obvious fluctuations of the temperature. During the fretting sliding, the temperature at the point increases as the pad begins to contacts with it, and decreases as the pad moves past the point.

Fig. 8(b) and (c) show the distributions of the temperature on the rough surface of the specimen after 1 cycle and 40 cycles, which are obtained with the consideration of the plastic dissipation and the friction dissipation, respectively. The influence of the plastic dissipation on the temperature rise is very different from that of the friction dissipation. The friction energy in each cycle nearly remains unchanged because the contact force and the slip displacement are constant. The continuous heat input from the friction dissipation causes the increase of the temperature, as shown in Fig. 8(a) and (c). However, the variation of the plastic dissipation between the first cycle and the subsequent cycles is significant. The temperature firstly exhibits a rapid increase and then decreases gradually. Through the comparison between Figs. 5 and 8, it is found that the plastic dissipation is needed to be considered in the simulation because the plastic energy has an important contribution for the increase of the temperature in the first cycle. However, the effect of the plastic dissipation on the temperature rise is insignificant in the subsequent cycles where the friction dissipation becomes the dominant heat input.

4.3. Effect of the surface roughness on the temperature rise

The temperature fields obtained under three conditions including two surface roughnesses ($R_a = 6$ and $12.5 \, \mu$m) and the smooth surface are compared to study the effect of the surface roughness. The other

(a)

(b)

(c)
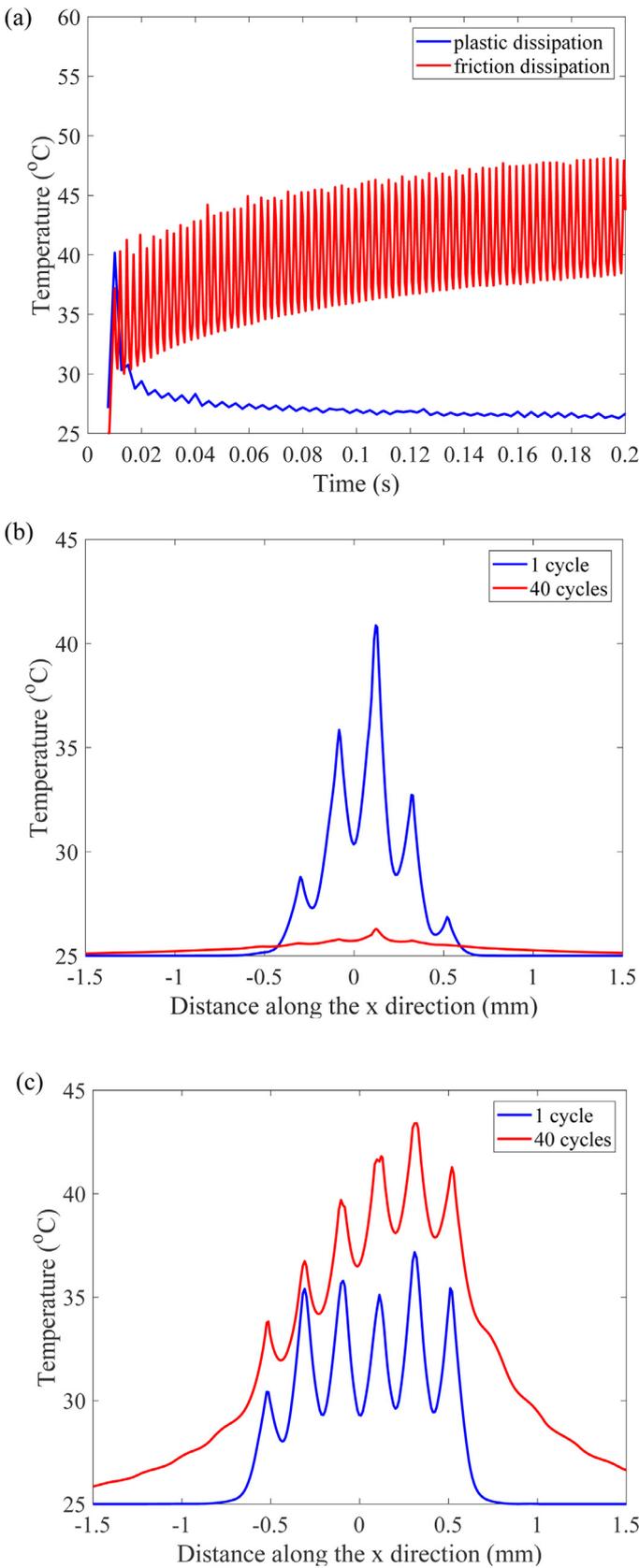
Fig. 8. (a) Evolutions of the temperature on the rough surface of the specimen obtained by two approaches considering the plastic dissipation and the friction dissipation respectively. Distributions of the temperature on the rough surface under the condition of considering only (b) the plastic dissipation and (c) the friction dissipation.

(a)

(b)
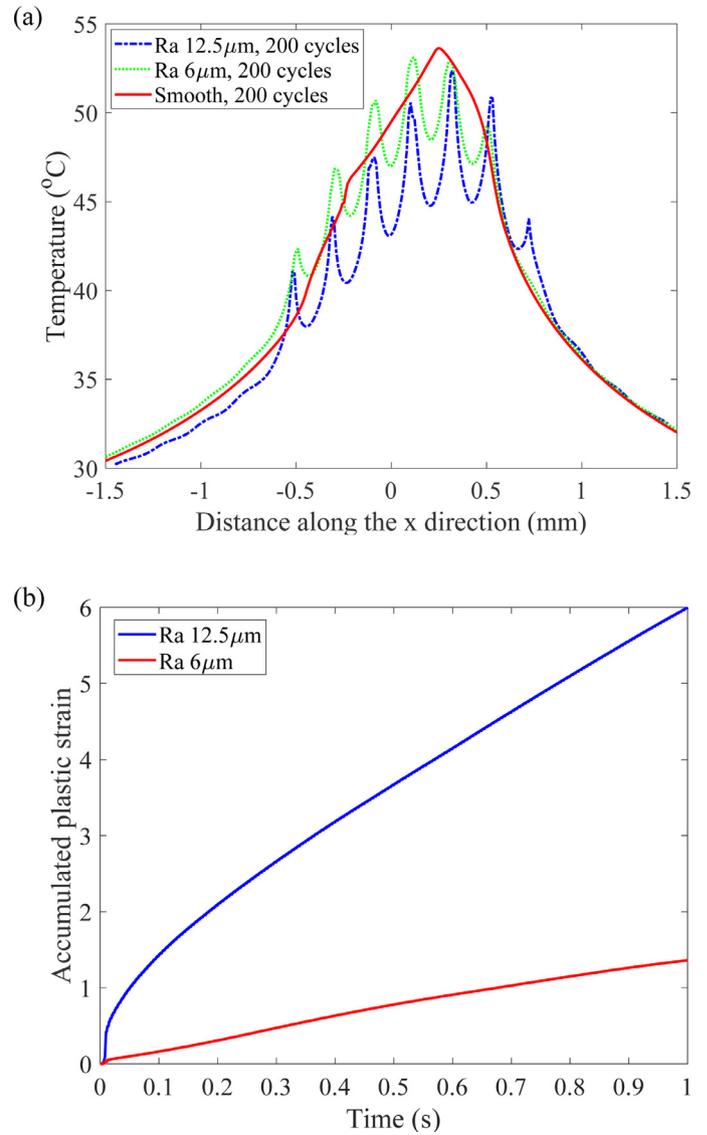
Fig. 9. (a) Distributions of the temperature on the contact surfaces after 200 cycles under the three conditions of surface roughnesses. (b) Evolutions of the accumulated plastic strain at the maximum temperature points on two rough surfaces.

conditions including the contact force, the slip displacement and the frequency remain unchanged. The friction dissipation, the plastic dissipation and the wear are all considered in the simulations.

Fig. 9(a) shows the distributions of the temperature on the contact surfaces after 200 cycles under the three conditions of surface roughnesses. The temperature distribution under the smooth surface condition shows a near-Hertzian shape. It is observed that the discrepancies on the values and the positions of three maximum temperature points are small. As mentioned in the previous subsection, the temperature rise after 200 cycles is mainly determined by the dissipation of the friction energy. The total friction energies generated on the contact surfaces are nearly identical because the contact force, the slip displacement, the co-efficient of friction and the cyclic stress on the specimen are the same under the three surface roughness conditions. Fig. 9(b) depicts the evolutions of the accumulated plastic strain at the maximum temperature points on two rough surfaces. The plastic deformation on the smooth contact surface is much smaller than the results in the figure. Larger plastic deformation occurs on the rougher surface. The linear increase of the plastic strain with the time follows a rapid increase in the first

several cycles. Even though the effect of the surface roughness on the plastic deformation is obvious, the variation of the plastic dissipation has insignificant influence on the temperature distribution after 200 cycles.

5. Conclusions

A numerical approach is developed to investigate the thermal response and the friction behavior in the Ti-6Al-4 V fretting sliding. The sliding of a cylindrical pad on a specimen with surface roughness is modeled in the coupled temperature-displacement finite element analysis to predict the distributions of the temperature rise, the wear profile, the surface stresses and the subsurface stresses in the contacting components. The thermo-elasto-plastic constitutive model, heat transfer model and modified Archard model are developed and incorporated in the modeling. The thermal-softening of the material properties and the plastic deformation are considered in the constitutive model. Both the friction and plastic dissipations function together as the heat source in the heat transfer model. The modified wear model takes the temperature-dependent wear coefficient into account.

The effect of the plastic dissipation on the temperature is reflected in the first several loading cycles, causing a rapid increase of the temperature. As the materials at the contacting peaks harden, the increment of the accumulated plastic in the subsequent cycle is about one order of magnitude less than that in the first cycle. Therefore, the effect of the plastic dissipation is insignificant and the friction dissipation becomes the dominant heat source in the subsequent cycles. The surface roughness affects the distributions of the contact pressure and the plastic strain on the contact surface. However, its effect on the temperature is not obvious after a number of loading cycles because the total friction energy is mainly determined by the loading conditions including the contact force and the slip displacement.

Acknowledgment

References

[1] Vingsbo O, Soderberg S. On fretting maps. Wear 1988;126:131–47.
[2] Hills DA, Nowell D. Mechanics of fretting fatigue. Oxford: Springer; 1994.
[3] Nowell D, Hills DA. Mechanics of fretting fatigue tests. Int J Mech Sci 1987;29:355–65.
[4] Cui XH, Mao YS, Wei MX, Wang SQ. Wear characteristics of Ti-6Al-4V Alloy at 20–400˚C. Tribol Trans 2012;55:185–90.
[5] Everitt NM, Ding J, Bandak G, Shipway PH, Leen SB, Williams EJ. Characterisation of fretting-induced wear debris for Ti-6Al-4V. Wear 2009;267:283–91.
[6] Warmuth AR, Shipway PH, Sun W. Fretting wear mapping: the influence of contact geometry and frequency on debris formation and ejection for a steel-on-steel pair. Proc R Soc A-Math Phys Eng Sci 2015;471:20140291.
[7] Jin X, Shipway PH, Sun W. The role of frictional power dissipation (as a function of frequency) and test temperature on contact temperature and the subsequent wear behaviour in a stainless steel contact in fretting. Wear 2015;330:103–11.
[8] Jin X, Sun W, Shipway PH. The role of geometry changes and debris formation associated with wear on the temperature field in fretting contacts. Tribol Int 2016;102:392–406.
[9] Hager CH, Sanders J, Sharma S, Voevodin A, Segall A. The effect of temperature on gross slip fretting wear of cold-sprayed nickel coatings on Ti6Al4V interfaces. Tribol Int 2009;42:491–502.
[10] Rybiak R, Fouvry S, Bonnet B. Fretting wear of stainless steels under variable temperature conditions: introduction of a 'composite'wear law. Wear 2010;268:413–23.
[11] Wang L, Zhang QY, Li XX, Cui XH, Wang SQ. Severe-to-mild wear transition of titanium alloys as a function of temperature. Tribol Lett 2014;53:511–20.
[12] Shen F, Hu W, Meng Q. A damage mechanics approach to fretting fatigue life prediction with consideration of elastic–plastic damage model and wear. Tribol Int 2015;82:176–90.
[13] Shen F, Hu WP, Voyiadjis GZ, Meng QC. Effects of fatigue damage and wear on fretting fatigue under partial slip condition. Wear 2015;338:394–405.
[14] Shen F, Hu WP, Meng QC. New approach based on continuum damage mechanics with simple parameter identification to fretting fatigue life prediction. Appl Math Mech-Engl Ed 2015;36:1539–54.
[15] Zhang T, McHugh PE, Leen SB. Computational study on the effect of contact geometry on fretting behaviour. Wear 2011;271:1462–80.
[16] Kalin M. Influence of flash temperatures on the tribological behaviour in low-speed sliding: a review. Mat Sci Eng A-Struct 2004;374:390–7.
[17] Kalin M, Vizintin J. Comparison of different theoretical models for flash temperature calculation under fretting conditions. Tribol Int 2001;34:831–9.
[18] Aghdam AB, Khonsari MM. Prediction of wear in reciprocating dry sliding via dissipated energy and temperature rise. Tribol Lett 2013;50:365–78.
[19] Wen J, Khonsari MM. Transient temperature involving oscillatory heat source with application in fretting contact. J Tribol-Trans ASME 2007;129:517–27.
[20] Pearson SR, Shipway PH, Abere JO, Hewitt RAA. The effect of temperature on wear and friction of a high strength steel in fretting. Wear 2013;303:622–31.
[21] Jaeger JC. Moving sources of heat and the temperature of sliding contacts. J Proc Roy Soc NSW 1942:203.
[22] Attia H. Thermal constriction phenomenon in fretting: theory and implications. Tribol Int 2011;44:1352–63.
[23] Qin W, Jin X, Kirk A, Shipway PH, Sun W. Effects of surface roughness on local friction and temperature distributions in a steel-on-steel fretting contact. Tribol Int 2018;120:350–7.
[24] Lu WL, Zhang P, Liva XJ, Zhai WZ, Zhou MZ, Luo J, Zeng WH, Jiang XQ. Influence of surface topography on torsional fretting wear under flat-on-flat contact. Tribol Int 2017;109:367–72.
[25] Kubiak KJ, Mathia TG, Fouvry S. Interface roughness effect on friction map under fretting contact conditions. Tribol Int 2010;43:1500–7.
[26] Horng JH, Wei CC, Tsai HJ, Shiu BC. A study of surface friction and particle friction between rough surfaces. Wear 2009;267:1257–63.
[27] Ovalle Rodas C, Zaïri F, Naït-Abdelaziz M. A finite strain thermo-viscoelastic constitutive model to describe the self-heating in elastomeric materials during low-cycle fatigue. J Mech Phys Solids 2014;64:396–410.
[28] Poncelet M, Doudard C, Calloch S, Weber B, Hild F. Probabilistic multiscale models and measurements of self-heating under multiaxial high cycle fatigue. J Mech Phys Solids 2010;58:578–93.
[29] Doudard C, Calloch S. Influence of hardening type on self-heating of metallic materials under cyclic loadings at low amplitude. Eur J Mech a-Solid 2009;28:233–40.
[30] Chaboche JL. A review of some plasticity and viscoplasticity constitutive theories. Int J Plast 2008;24:1642–93.
[31] Kang GZ, Liu YJ, Ding J, Gao Q. Uniaxial ratcheting and fatigue failure of tempered 42CrMo steel: damage evolution and damage-coupled visco-plastic constitutive model. Int J Plast 2009;25:838–60.
[32] Sun Y, Hu WP, Shen F, Meng QC, Xu YM. Numerical simulations of the fatigue damage evolution at a fastener hole treated by cold expansion or with interference fit pin. Int J Mech Sci 2016;107:188–200.
[33] Zhan ZX, Hu WP, Li BK, Zhang YJ, Meng QC, Guan ZD. Continuum damage mechanics combined with the extended finite element method for the total life prediction of a metallic component. Int J Mech Sci 2017;124:48–58.
[34] Lemaitre J, Chaboche JL. Mechanics of solid materials. Cambridge: Cambridge University Press; 1994.
[35] McColl IR, Ding J, Leen SB. Finite element simulation and experimental validation of fretting wear. Wear 2004;256:1114–27.
[36] Ding J, McColl IR, Leen SB, Shipway PH. A finite element based approach to simulating the effects of debris on fretting wear. Wear 2007;263:481–91.
[37] Kasarekar AT, Bolander NW, Sadeghi F, Tseregounis S. Modeling of fretting wear evolution in rough circular contacts in partial slip. Int J Mech Sci 2007;49:690–703.
[38] Mattei L, Di Puccio F. Influence of the wear partition factor on wear evolution modelling of sliding surfaces. Int J Mech Sci 2015;99:72–88.
[39] Jin O, Mall S. Effects of independent pad displacement on fretting fatigue behavior of Ti–6Al–4V. Wear 2002;253:585–96.
[40] Jin O, Mall S. Effects of slip on fretting behavior: experiments and analyses. Wear 2004;256:671–84.
[41] Hager Jr CH, Sanders JH, Sharma S. Unlubricated gross slip fretting wear of metallic plasma-sprayed coatings for Ti6Al4V surfaces. Wear 2008;265:439–51.
[42] Yang J, Sun S, Brandt M, Yan W. Experimental investigation and 3D finite element prediction of the heat affected zone during laser assisted machining of Ti6Al4V alloy. J Mater Process Technol 2010;210:2215–22.
[43] Handbook M. MIL-HDBK-5H: metallic materials and elements for aerospace vehicle structures. US Department of Defense; 1998.